Supporting Information:

Discovery of Two-Dimensional Binary Nanoparticle Superlattices Using Global Monte Carlo Optimization

Yilong Zhou and Gaurav Arya*

Department of Mechanical Engineering and Materials Science, Duke University,

Durham, North Carolina 27708, United States

* Corresponding author

Email: gaurav.arya@duke.edu, Phone: +1 (919) 660-5435, Fax: +1 (919) 660-8963

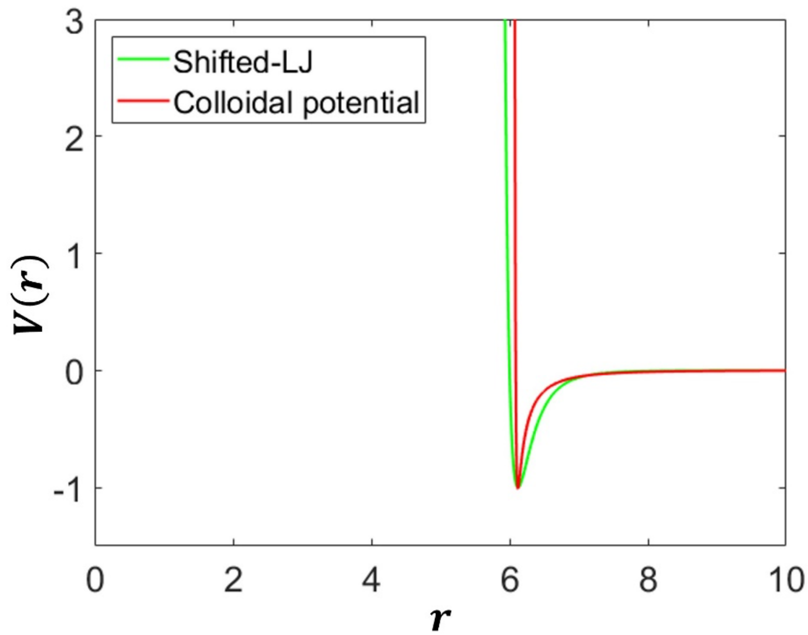

Figure S1. Comparison of the shifted-LJ potential used in this work and the inter-colloidal vdW interaction potential for silica NPs of size $R = 3$ nm. The energies in both potentials are normalized by the magnitude of the potential energy minimum.

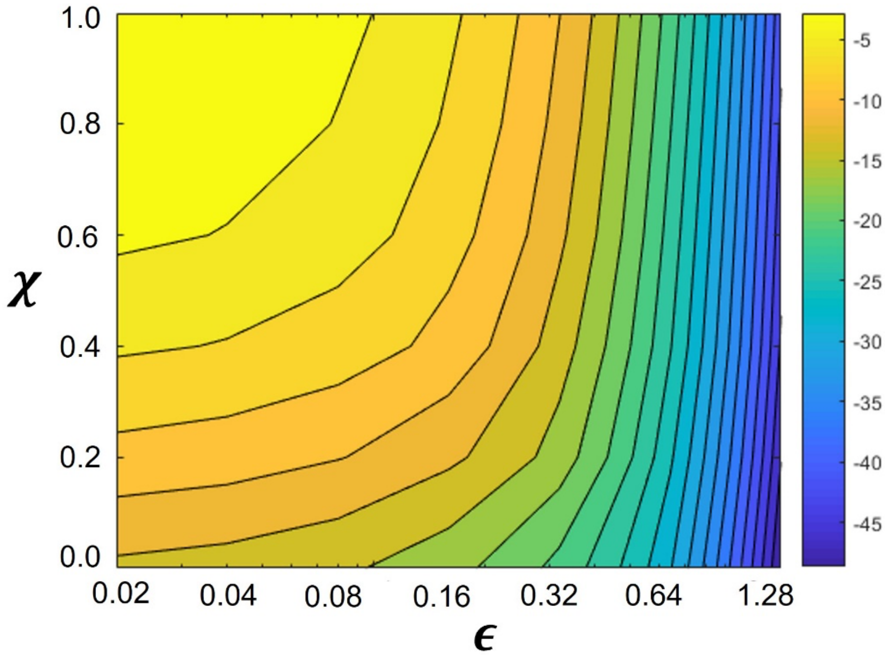

Figure S2. Contour map of the total energy E_{tot} of the minimum-energy NP configurations depicted in Figure 2A.

Table S1. Comparison of the total energy of NP structures predicted by our analytical model for various monolayer, bilayer, and globular phases.

Structural Phases		$\boldsymbol{m}$	$\boldsymbol{n}$	$\boldsymbol{E_{\mathrm{tot}}}$
SP1	**SP2**			
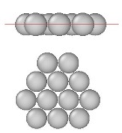	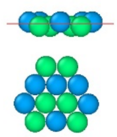	12	24	$-m(1-\chi)^2$ $-\ n\epsilon$
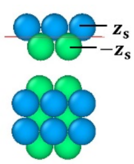	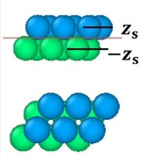	$\frac{12\left\{-\left(1-\left(\frac{z_s}{R}\right)^2\right)+2\left(1-\frac{z_s}{R}\right)\chi\right\}}{-(1-\chi)^2}$ (SP1: $z_s = 2.16\sigma$ SP2: $z_s = 2.5\sigma$)	SP1: $n = 30$ SP2: $n = 31$	
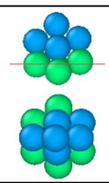	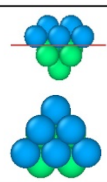	SP1: $\bar{m} \approx 6.5$ SP2: $\bar{m} \approx 4.5$	33	

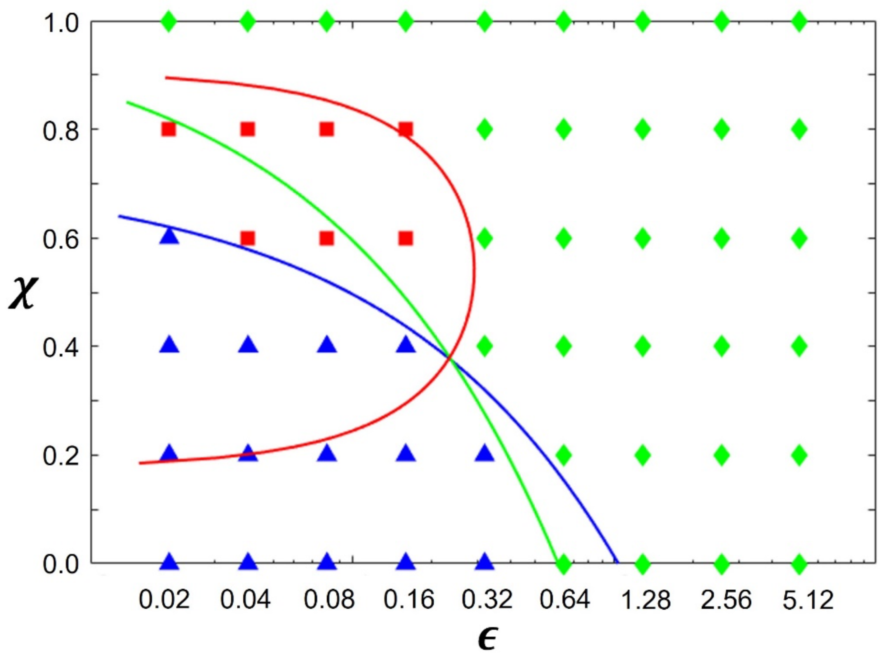

Figure S3. Boundaries between monolayer, bilayer, and globular phases predicted by our analytical model based on the analysis of m and n of the corresponding structures. The boundaries between the monolayer and bilayer phases, the monolayer and globular phases, and the bilayer and globular phases are shown by blue, green, and red lines, respectively.

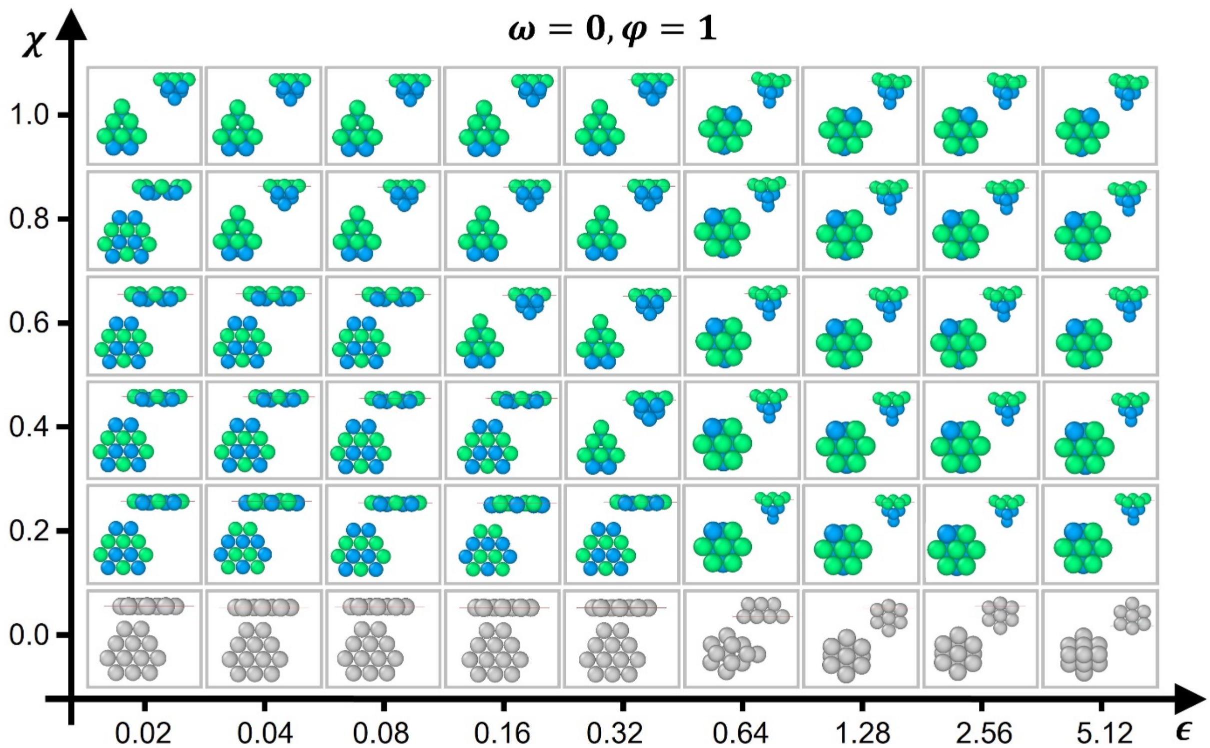

Figure S4. Structural phase diagram of 6:6 NPs (top and side views) at $\omega = 0$ and $\varphi = 1$ with respect to the interparticle interaction strength parameter ϵ and the relative miscibility parameter χ.

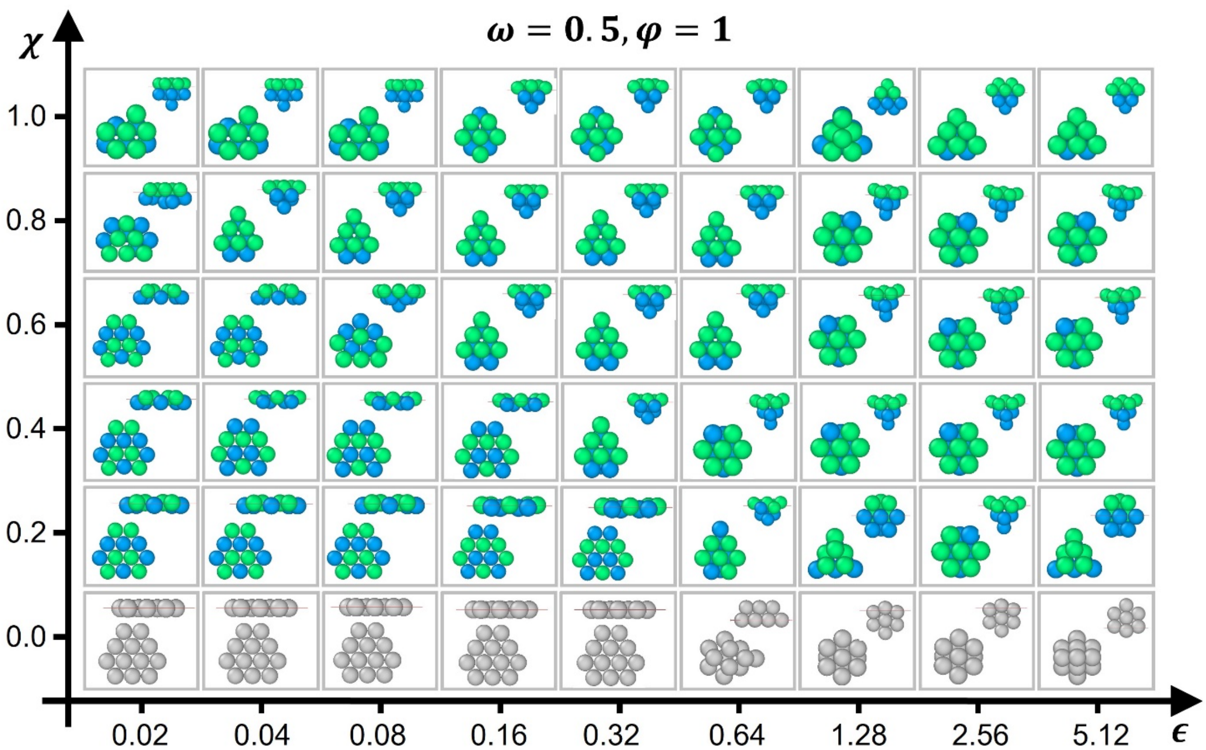

Figure S5. Structural phase diagram of 6:6 NPs (top and side views) at $\omega = 0.5$ and $\varphi = 1$ with respect to the interparticle interaction strength parameter ϵ and relative miscibility parameter χ.

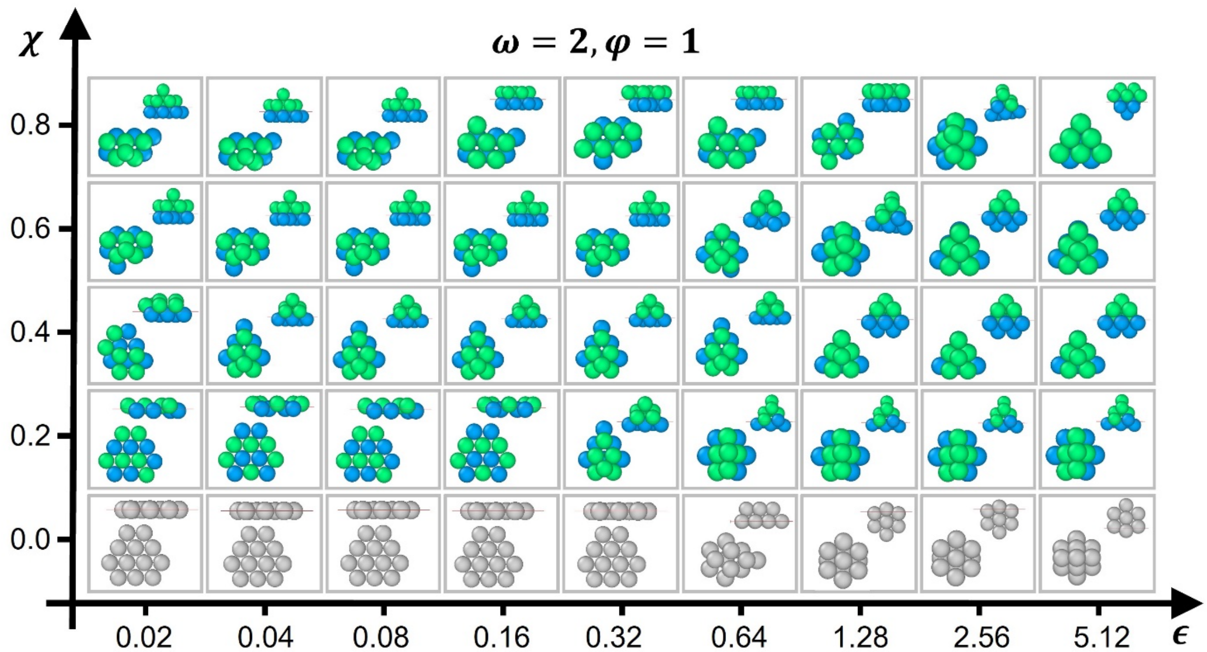

Figure S6. Structural phase diagram of 6:6 NPs (top and side views) at $\omega = 2$ and $\varphi = 1$ with respect to interparticle interaction strength parameter ϵ and relative miscibility parameter χ.

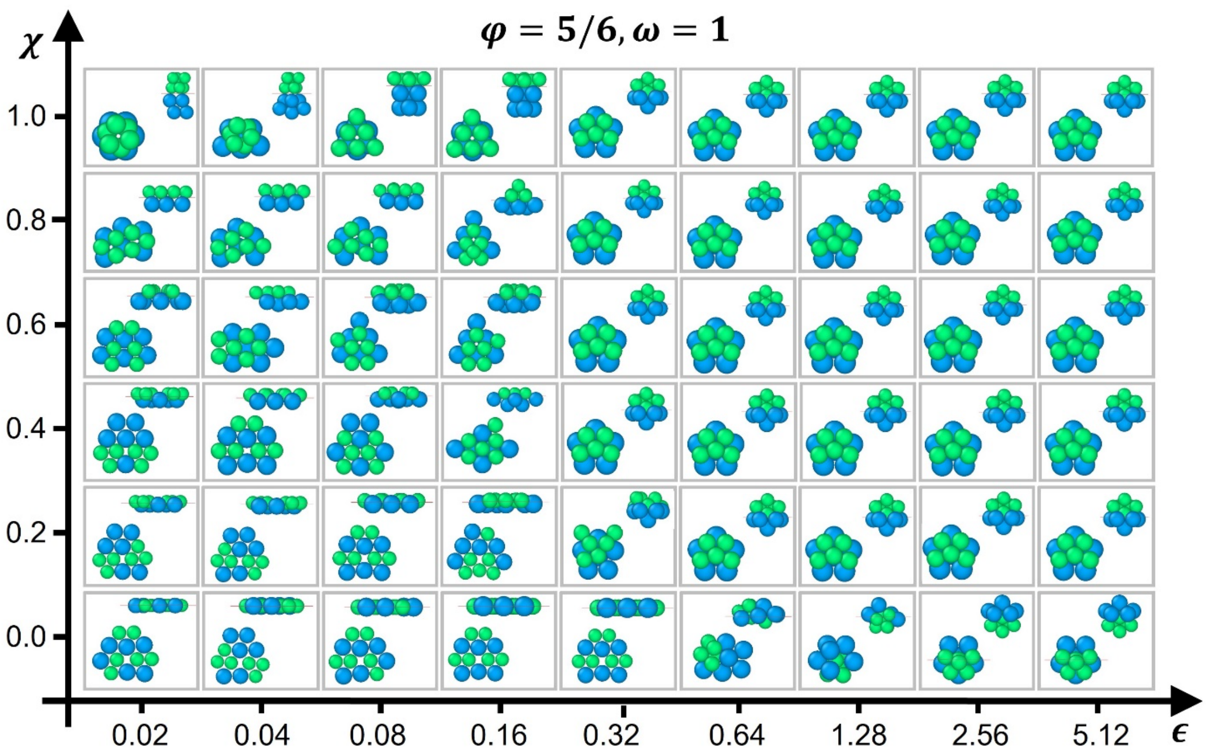

Figure S7. Structural phase diagram of 6:6 NPs (top and side views) at $\varphi = 5/6$ and $\omega = 1$ with respect to interparticle interaction strength parameter ϵ and relative miscibility parameter χ.

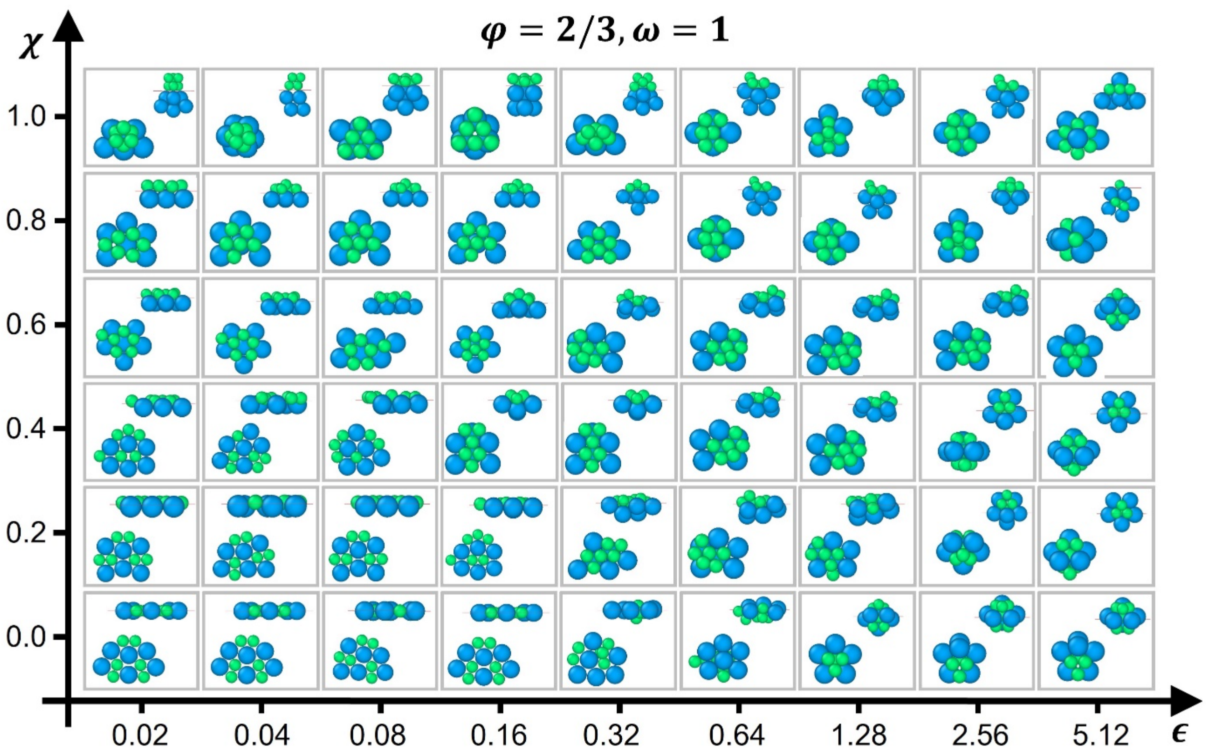

Figure S8. Structural phase diagram of 6:6 NPs (top and side views) at $\varphi = 2/3$ and $\omega = 1$ with respect to interparticle interaction strength parameter ϵ and relative miscibility parameter χ.

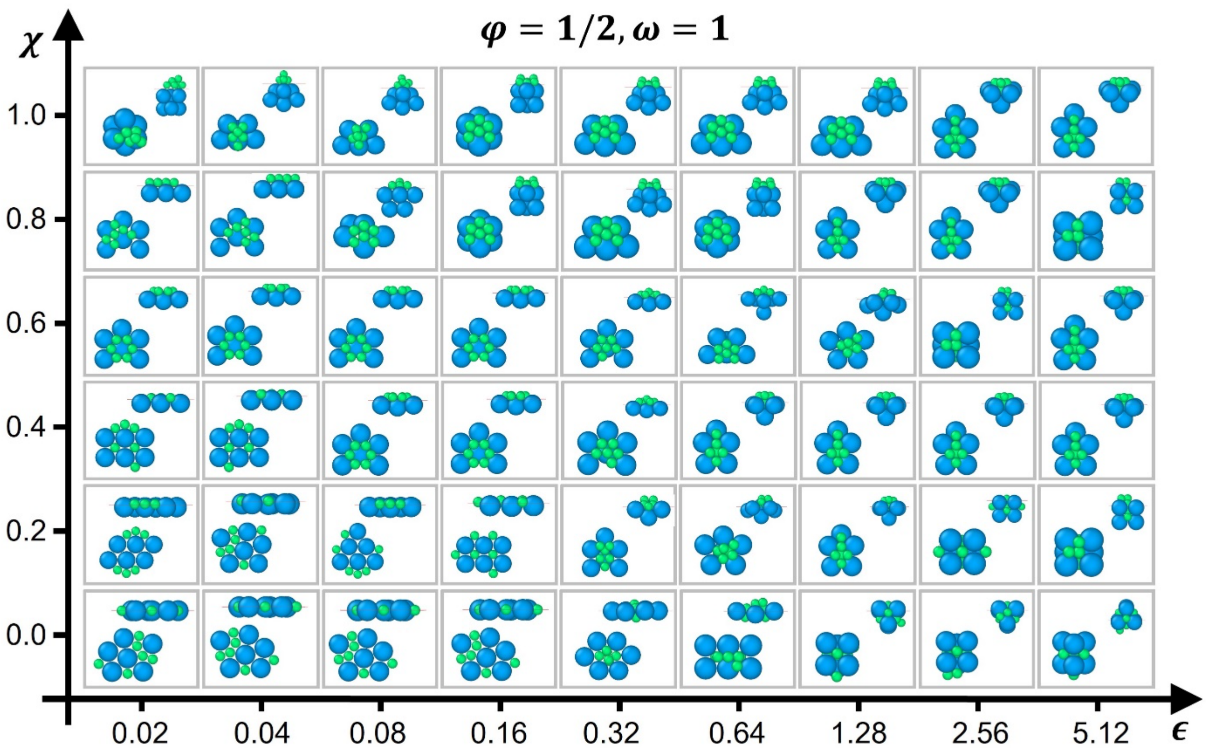

Figure S9. Structural phase diagram of 6:6 NPs (top and side views) at $\varphi = 1/2$ and $\omega = 1$ with respect to interparticle interaction strength parameter ϵ and relative miscibility parameter χ.

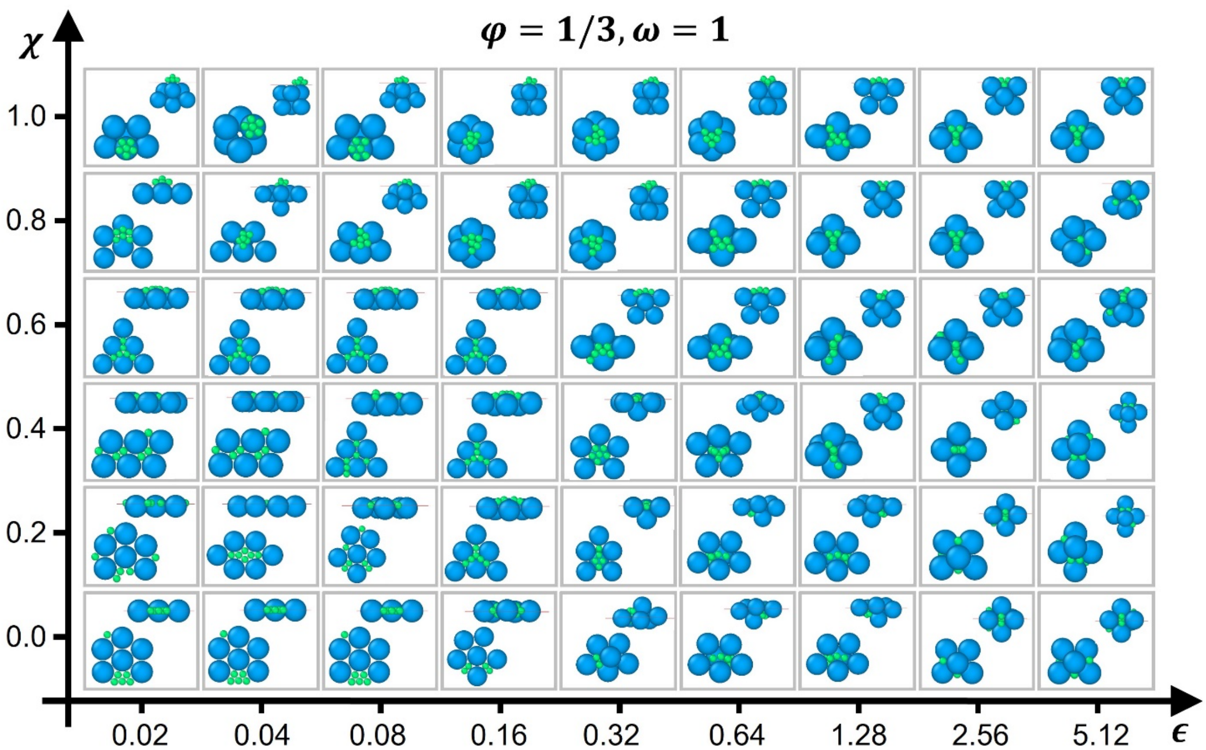

Figure S10. Structural phase diagram of 6:6 NPs (top and side views) at $\varphi = 1/3$ and $\omega = 1$ with respect to interparticle interaction strength parameter ϵ and relative miscibility parameter χ.

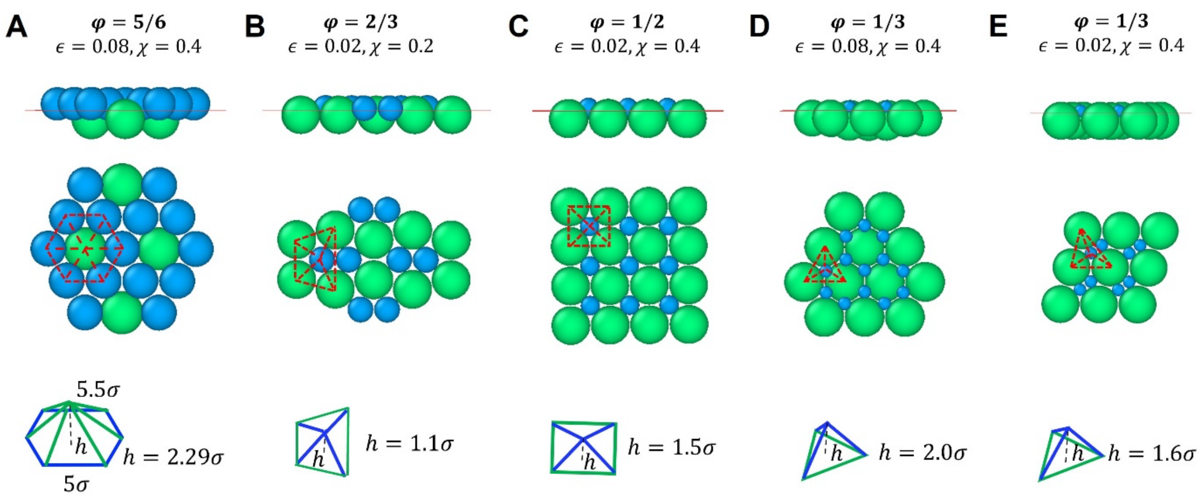

Figure S11. Monolayer BNSLs obtained at different particle size ratios. (A) AB_3-type BNSL with hexagonal order at $\varphi = 5/6$. (B) AB-type BNSL with stretched hexagonal order at $\varphi = 2/3$. (C) AB-type BNSL with square order at $\varphi = 1/2$. (D) AB_2-type BNSL with triangular order at $\varphi = 1/3$. (E) AB_2-type BNSL with rhombic order at $\varphi = 1/3$. The schematics at the bottom show the arrangement of one species of NPs around the other species. The vertical heights of the pyramids denoted by h provides the spacing between the two layers of NPs (in the direction normal to the interfacial plane).

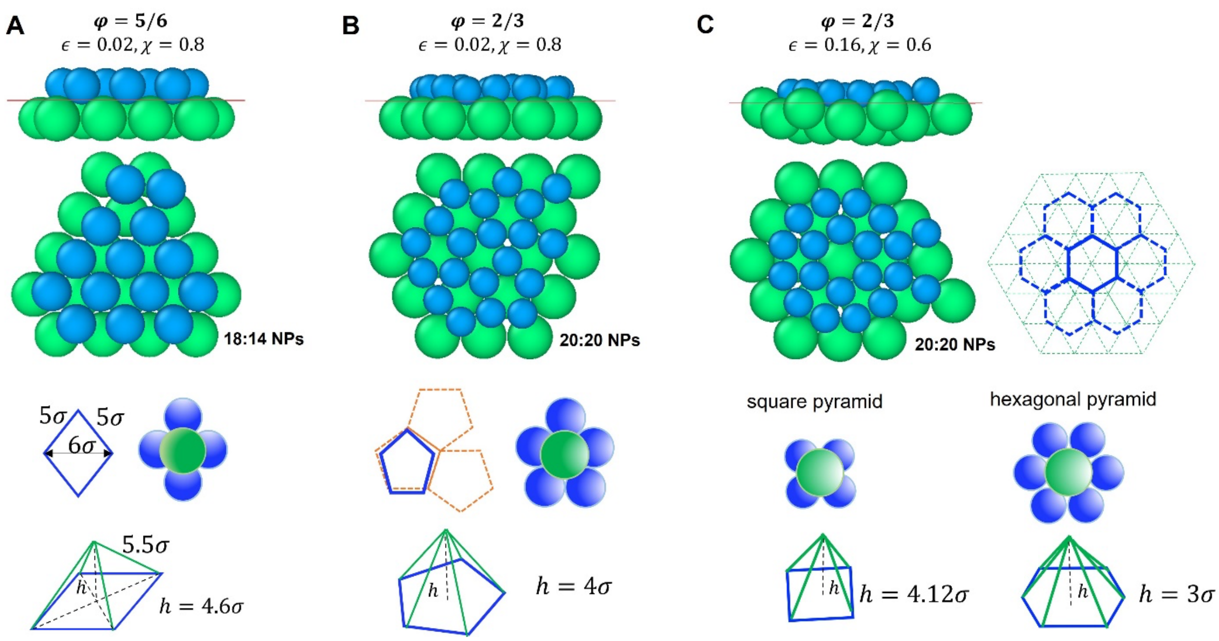

Figure S12. Hybrid bilayer BNSLs obtained at different particle size ratios showing how small NPs form unique quasi-periodic and periodic layers atop a hexagonally ordered sheet of large NPs. (A) AB-type BNSL with a quasi-periodic rhombic ordering of small NPs obtained at $\varphi = 5/6$. (B) A_3B_5-type BNSL with a periodic pentagonal-triangular arrangement of small NPs at $\varphi = 2/3$. Regular pentagons are unable to form a periodic tessellation, as schematically shown by the three pentagons in dashed brown lines. (C) A_4B_6-type BNSL made of periodic hexagonal, square, and triangular motifs at $\varphi = 2/3$. That hexagons on their own are unable to form a periodic arrangement on the hexagonally arranged lattice is schematically shown by blue and green dashed lines. In all cases, the NP numbers were deliberately chosen to be incompatible with the number of NPs in a unit cell to demonstrate robustness of the observed structures. The schematics at the bottom show the arrangement of one species of NPs atop the other species. The vertical heights of the pyramids, denoted by h, provide the spacing between the two layers of NPs.